Journal of Alloys and Compounds 495 (2010) 55–58

Contents lists available at ScienceDirect

Journal of Alloys and Compounds

journal homepage: www.elsevier.com/locate/jallcom

The effects of secondary elemental Mo or Ti addition in $Al_{0.3}CoCrFeNi$ high-entropy alloy on age hardening at 700 °C

Tao-Tsung Shun*, Cheng-Hsin Hung, Che-Fu Lee

Department of Materials Science and Engineering, Feng Chia University, 100 Wenhwa Rd., Seatwen, Taichung 407, Taiwan

ARTICLE INFO

Article history:
Received 12 December 2009
Accepted 6 February 2010
Available online 16 February 2010

Keywords:
High-entropy alloy
Enthalpy
Microstructure
Crystal structure
Transmission electron microscopy

ABSTRACT

Three FCC structured high-entropy alloys of $Al_{0.3}CoCrFeNi$, $Al_{0.3}CoCrFeNiMo_{0.1}$, and $Al_{0.3}CoCrFeNiTi_{0.1}$ were synthesized in order to investigate the effects of secondary elemental Mo or Ti addition in $Al_{0.3}CoCrFeNi$ alloy on age hardening at 700 °C. All of the three alloys exhibited an apparent age hardening, especially when secondary elements were added. The hardness of the $Al_{0.3}CoCrFeNi$ alloy was increased by 65% after aging, whereas the other two alloys displayed an increase of over 80%. The $Al_{0.3}CoCrFeNi$ and $Al_{0.3}CoCrFeNiTi_{0.1}$ alloys were hardened by massive (Ni,Al)-rich and (Ni,Co,Ti)-rich B2 ordered precipitates, respectively. The large age hardening of the $Al_{0.3}CoCrFeNiMo_{0.1}$ alloy is attributed to the precipitation of both fine (Ni,Al)-rich phase and heavy blocky (Cr,Mo)(Co,Fe,Ni) σ phase.

1. Introduction

New alloy systems constructed by multi-principal elements, termed high-entropy alloys, were proposed by Yeh et al. in 2004 [1]. A high-entropy alloy was defined as an alloy which contained at least 5 principal elements, each with concentrations between 5 at.% and 35 at.%. The characteristic of high mixing entropy ΔS_{mix} of an alloy with multi-principal elements facilitates the formation of simple solid solutions during solidification instead of complex phases or inter-metallic compounds [1–4]. The Al–Co–Cr–Cu–Fe–Ni alloys have been widely studied on microstructures and mechanical properties [5–11]. Except for the segregation of Cu in interdendritic regions, the crystal structure of alloys displayed simple FCC and/or BCC solid solutions depending on the concentrations of each principal element. The crystal structure of $Al_xCoCrCuFeNi$ alloys was transformed from FCC to BCC as the aluminum content was increased. They exhibited good high-temperature strengths up to 800 °C [6]. For the AlCoCrCuFeNi alloy [10], a decrease of yield strength with increasing aging temperature above 645 °C was observed due to the structural change from a stabilized BCC to FCC. In the studies of Al–Co–Cr–Fe–Ni–Ti alloy systems [3,12–15], the strong BCC solid solutions or mixed Laves phases demonstrated excellent room-temperature compressive strengths that were superior to most bulk metallic glasses. At present, most researchers concentrate on the variety of principal elements in high-entropy alloys to investigate novel microstructures and properties. However, the effects of secondary elemental additions are seldom reported.

In our previous work regarding the age hardening of adding secondary element C in $Al_{0.3}CoCrFeNi$ alloy, the $Al_{0.3}CoCrFeNiC_{0.1}$ alloy appeared the strongest age hardening at 700 °C due to the precipitation of fine k_2 carbides [16]. In this paper, the effects of secondary elemental Mo or Ti addition in $Al_{0.3}CoCrFeNi$ alloy on the microstructure and age hardening at 700 °C were studied.

2. Experimental methods

Three high-entropy alloys with a nominal chemical composition of $Al_{0.3}CoCrFeNi$, $Al_{0.3}CoCrFeNiMo_{0.1}$, and $Al_{0.3}CoCrFeNiTi_{0.1}$ (named A-0, A-0.1Mo, and A-0.1Ti, respectively) were synthesized by arc melting under a Ti-gettered high-purity argon atmosphere in a water-cooled copper crucible. Elemental Al, Co, Cr, Fe, Ni, Mo, and Ti with 99 wt.% purity were used as raw materials. The ingot was melted 4 times to ensure homogeneity. The size of the ingot was approximately 60 mm × 40 mm × 10 mm. Samples cut from the ingot were heat treated for 24, 72, and 144 h at 700 °C, and individually quenched in water. Hardness measurements, phase identification, and microstructure analyses were then carried out on the as-cast and aged specimens. The hardness was measured using a Vickers hardness tester. Measurement was made by an average of seven points. The crystal structures were characterized using X-ray diffractometer (XRD) with Cu Kα radiation scanning from 20° to 100° degrees in 2θ at a scanning rate of 2°/min. The microstructure and chemical composition were examined using scanning electron microscopy (SEM) equipped with an energy dispersive spectrometer (EDS). Thin foils were used for detailed phase identification using transmission electron microscopy (TEM).

3. Results and discussion

3.1. The as-cast alloys

The XRD patterns and hardness of the three as-cast alloys are shown in Fig. 1. All alloys display a single FCC solid solution and

* Corresponding author. Tel.: +886 4 24517250x5308; fax: +886 4 24510014.
E-mail address: ttshun@fcu.edu.tw (T.-T. Shun).

0925-8388/$ – see front matter © 2010 Elsevier B.V. All rights reserved.
doi:10.1016/j.jallcom.2010.02.032

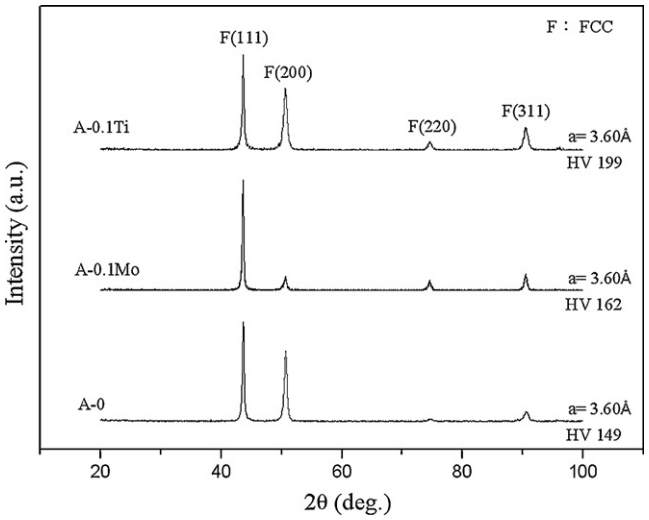

Fig. 1. XRD patterns and hardness of the three as-cast alloys.

Table 1
The mixing enthalpy of atom pair between each element (KJ/mole) [18].

	Al	Co	Cr	Fe	Ni	Mo	Ti
Al	0	−19	−10	−11	−22	−5	−30
Co		0	−4	−1	0	−5	−28
Cr			0	−1	−7	0	−7
Fe				0	−2	−2	−17
Ni					0	−7	−35
Mo						0	−4
Ti							0

their lattice constants are estimated to be 3.60 Å by extrapolating the calculations of four diffraction peaks [17]. A small amount of Mo or Ti addition did not create a change in the lattice constant, but could moderately raise hardness due to solid solution strengthening. The addition of the relatively large atom, Ti (atomic radius 1.47 Å) yielded a more significant strengthening effect due to the greater lattice distortion.

Fig. 2 shows SEM images of the as-cast A-0 and A-0.1Mo alloys. The A-0 alloy exhibits a crystalline structure and no significant compositional segregation occurs. The A-0.1Mo alloy presents a dendritic structure. However, the EDS analyses show that compositional segregation in the dendrite and interdendrite regions is not very significant during solidification. The SEM images of the as-cast A-0.1Ti alloy shown in Fig. 3 also present a dendritic structure, in which the interdendrite is enriched by Ni, Co, Al, and Ti in comparison with the dendrite. This is due to the mixing enthalpies of relatively electronegative elements (Ni and Co) with more electropositive elements (Al and Ti) being much more negative than for other atomic pairs present. Table 1 lists the mixing entropy of atom pairs. The TEM microstructure shown in Fig. 4 shows that the interdendrite has a HCP crystal structure.

3.2. The aged alloys

3.2.1. The variations of hardness and crystal structure

Fig. 5 shows the variations in hardness of the alloys aged at 700 °C. Each alloy exhibits good age hardening, especially the A-0.1Mo alloy. The hardness of A-0, A-0.1Mo, and A-0.1Ti alloys increased by 65%, 89%, and 83%, respectively, after 144 h of aging. Fig. 6 shows the XRD patterns of the alloys after aging for 144 h. When comparing with Fig. 1, the crystal structures of A-0, A-0.1Mo, and A-0.1Ti alloys changed to FCC + BCC, FCC + BCC + σ, and FCC + BCC, respectively. Fig. 5 indicates that both A-0 and A-0.1Ti alloys are hardened by the precipitation of a BCC phase, and the A-0.1Mo alloy is hardened significantly by the precipitation of both the BCC and σ phases.

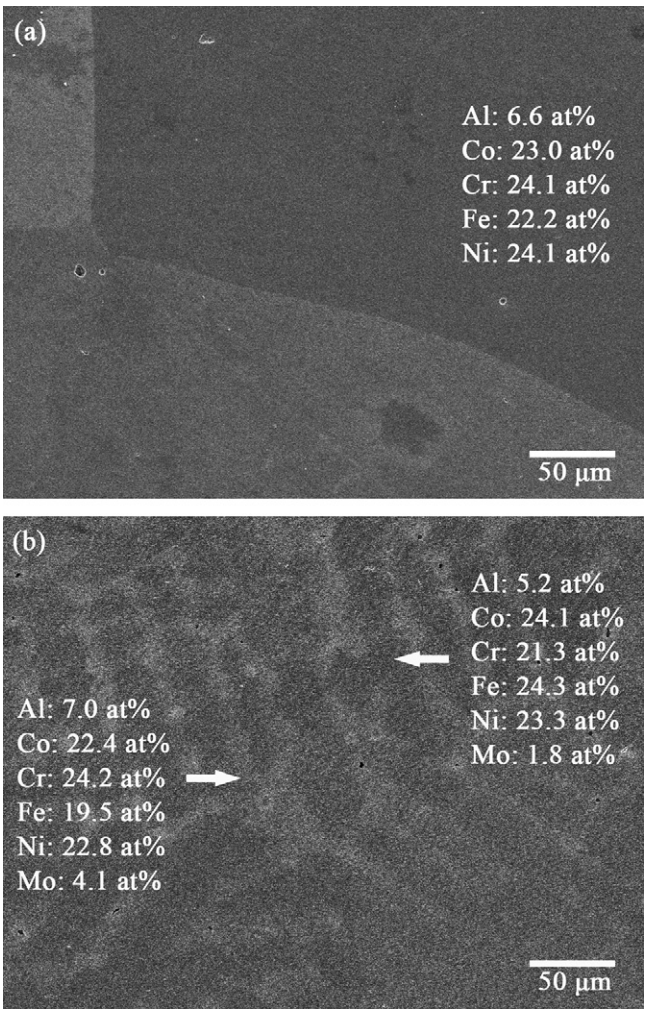

Fig. 2. SEM images of the as-cast A-0 and A-0.1Mo alloys.

3.2.2. Microstructure characterization

An SEM image of the A-0 alloy is shown in Fig. 7. There are massive (Ni,Al)-rich precipitates that formed in the matrix. From the results of the XRD pattern in Fig. 6 and in our previous report [19], these precipitates are suggested to be a B2 ordered structure and explain the age hardening. The microstructure of the A-0.1Mo alloy shown in Fig. 8 exhibits heavy blocky Cr-rich precipitates in addition to the fine (Ni,Al)-rich precipitates. This Cr-rich precipitate, corresponding to stoichiometric (Cr,Mo)(Co,Fe,Ni), is a σ phase that was detected by XRD, as shown in Fig. 6. According to the electron hole theory applied to superalloys [20], it is believed that Mo is a key element of σ phase formation since it has a larger electron hole number N_v than most transition elements. It is well recognized that the hard σ is one of the TCP phases which significantly disrupt alloy properties on fracture initiation and propagation due to a plate-like or needle-like morphology; however, the massive σ with a blocky structure might affect properties positively. For A-0.1Mo alloy, the dual precipitates of a (Ni,Al)-rich B2 phase and a σ phase results in a large level of age hardening.

Fig. 9 is a SEM image of the A-0.1Ti alloy. Large amounts of precipitate are observed and their morphologies are similar to the precipitates found in the A-0 alloy. However, these precipitates are

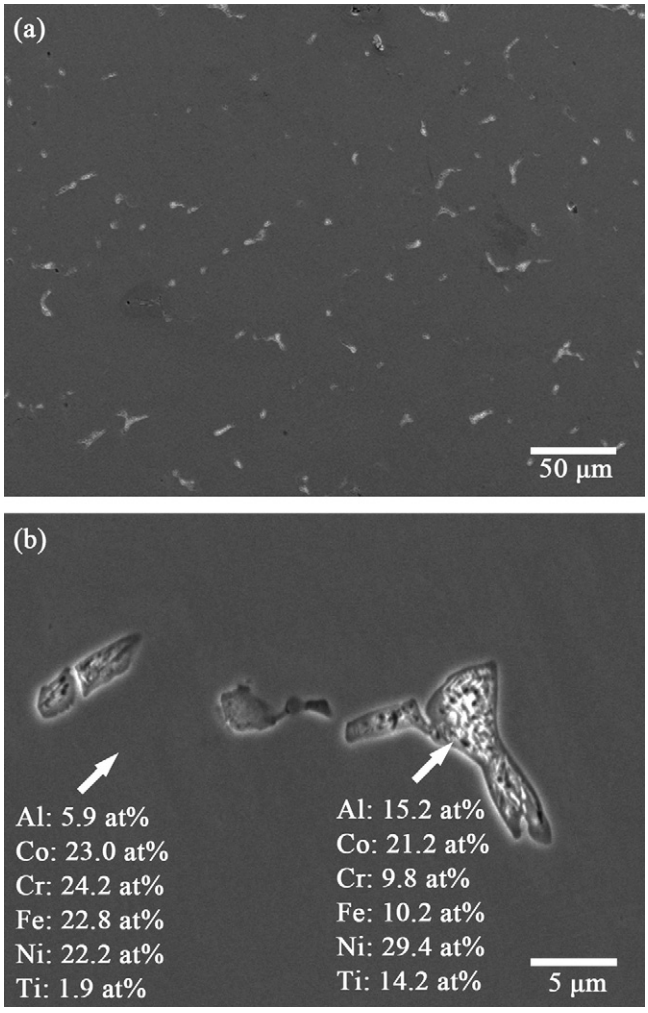

Fig. 3. SEM images of the as-cast A-0.1Ti alloy: (a) low magnification and (b) high magnification.

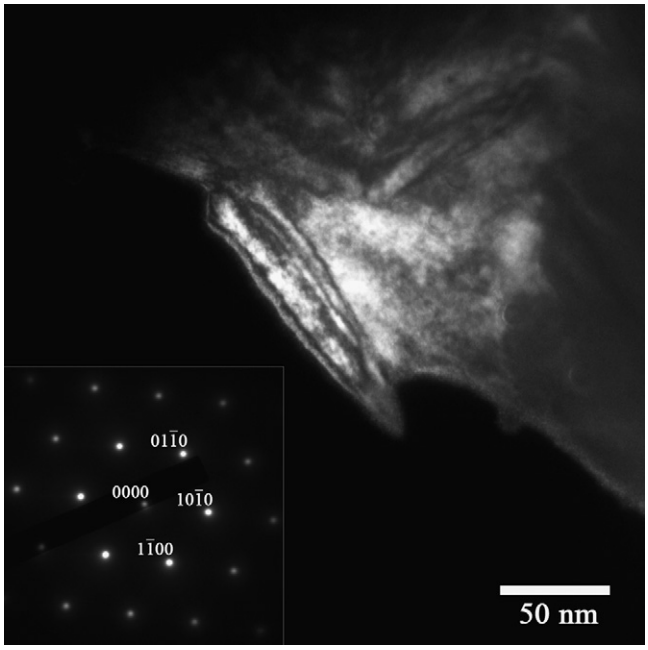

Fig. 4. TEM microstructure of the interdendrite region in the A-0.1Ti alloy: dark-field image corresponding to (0 1 $\bar{1}$ 0) spot from a selected area diffraction pattern of the HCP [0 0 0 1] zone axis.

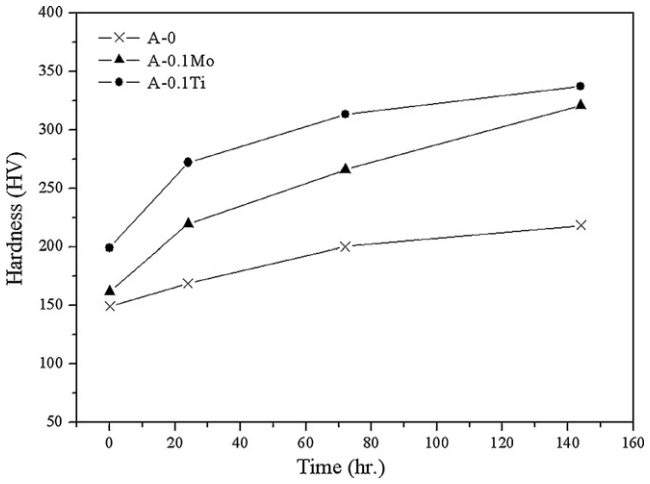

Fig. 5. The variations in hardness of the alloys aged at 700 °C.

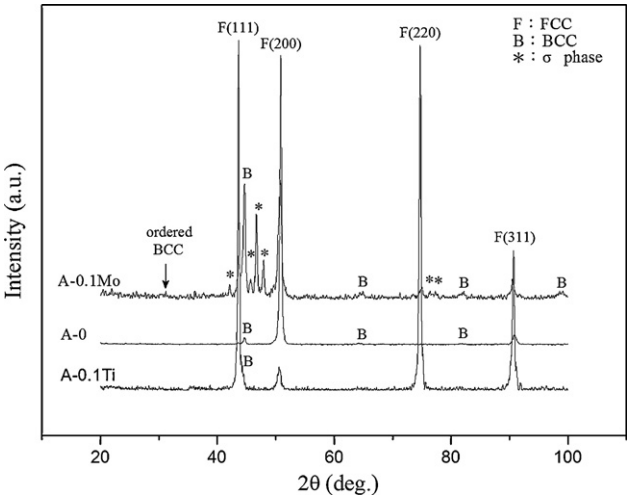

Fig. 6. XRD patterns of the alloys aged at 700 °C for 144 h.

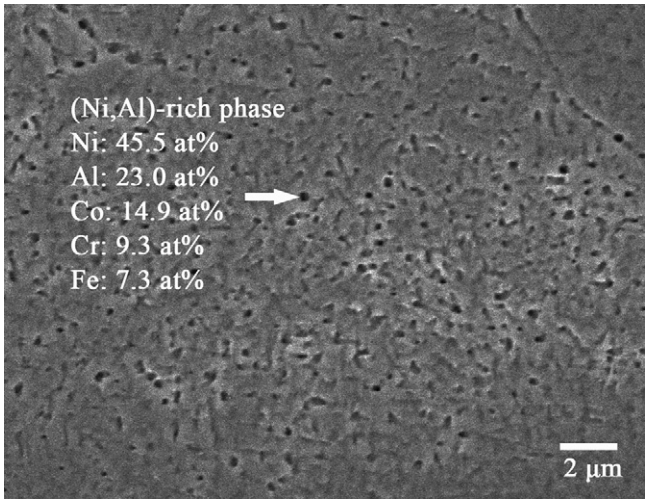

Fig. 7. SEM image of the aged A-0 alloy.

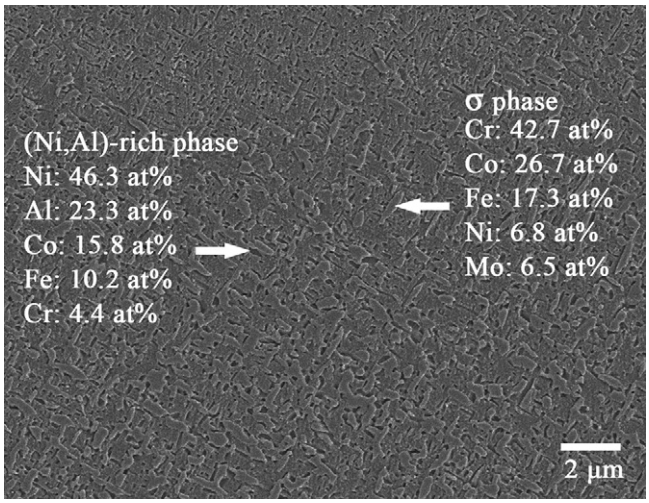

Fig. 8. SEM image of the aged A-0.1Mo alloy.

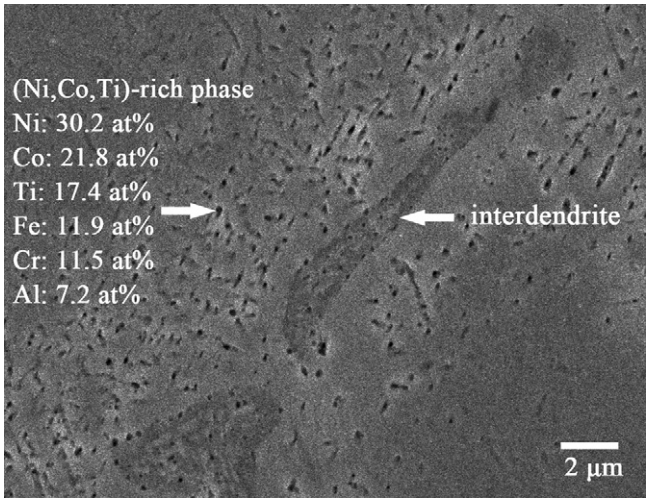

Fig. 9. SEM image of the aged A-0.1Ti alloy.

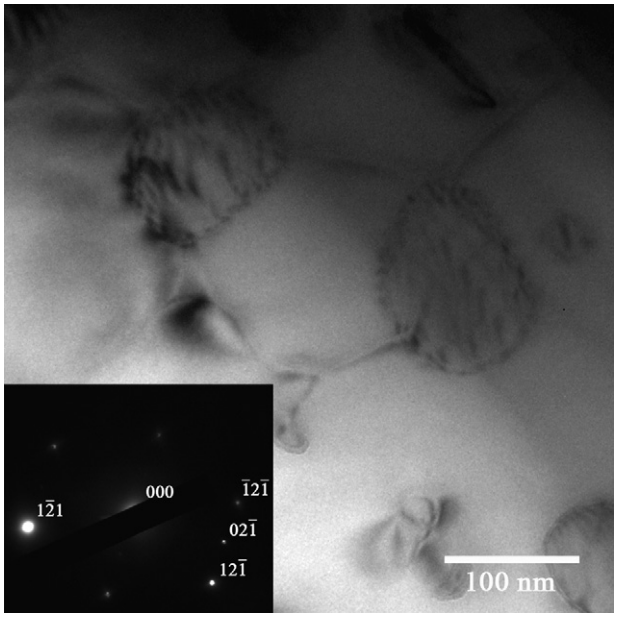

Fig. 10. TEM microstructure of the aged A-0.1Ti alloy: bright-field image with a selected area diffraction pattern of the BCC [0 1 2] zone axis.

rich in Ni, Co, and Ti. The higher negative mixing enthalpies of Ni–Ti and Co–Ti led to the formation of a (Ni,Co,Ti)-rich precipitate. The TEM microstructure shown in Fig. 10 reveals that this precipitate possesses a B2 ordered structure. Therefore, the age hardening of the A-0.1Ti alloy is attributed to the precipitation of a (Ni,Co,Ti)-rich B2 phase.

4. Conclusions

Three FCC structured high-entropy alloys, $Al_{0.3}CoCrFeNi$, $Al_{0.3}CoCrFeNiMo_{0.1}$, and $Al_{0.3}CoCrFeNiTi_{0.1}$, underwent apparent age hardening at 700 °C and hardness increases of 65–89% were observed after 144 h of aging. The precipitations of a (Ni,Al)-rich B2 phase in $Al_{0.3}CoCrFeNi$ alloy and a (Ni,Co,Ti)-rich B2 phase in $Al_{0.3}CoCrFeNiTi_{0.1}$ alloy result in age hardening. The dual precipitates of a (Ni,Al)-rich phase and a (Cr,Mo)(Co,Fe,Ni) σ phase explain the significant age hardening of the $Al_{0.3}CoCrFeNiMo_{0.1}$ alloy.

References

[1] J.W. Yeh, S.K. Chen, J.Y. Gan, T.S. Chin, T.T. Shun, C.H. Tsau, S.Y. Chang, Adv. Eng. Mater. 6 (5) (2004) 299–303.
[2] Y.J. Zhou, Y. Zhang, Y.L. Wang, G.L. Chen, Appl. Phys. Lett. 90 (2007) 181904.
[3] Y. Zhang, Y.J. Zhou, J.P. Lin, G.L. Chen, P.K. Liaw, Adv. Eng. Mater. 10 (6) (2008) 534–538.
[4] A. Li, X. Zhang, Acta Metall. Sin. (Engl. Lett.) 22 (3) (2009) 219–224.
[5] C.C. Tung, J.W. Yeh, T.T. Shun, S.K. Chen, Y.S. Huang, H.C. Chen, Mater. Lett. 61 (2007) 1–5.
[6] C.J. Tong, M.R. Chen, S.K. Chen, J.W. Yeh, T.T. Shun, S.J. Lin, S.Y. Chang, Metall. Mater. Trans. A 36A (2005) 1263–1271.
[7] C.J. Tong, M.R. Chen, S.K. Chen, J.W. Yeh, T.T. Shun, S.J. Lin, S.Y. Chang, Metall. Mater. Trans. A 36A (2005) 881–893.
[8] J.M. Wu, S.J. Lin, J.W. Yeh, S.K. Chen, Y.S. Huang, H.C. Chen, Wear 261 (2006) 513–519.
[9] Y.J. Zhou, Y. Zhang, F.J. Wang, G.L. Chen, Appl. Phys. Lett. 92 (2008) 241917.
[10] L.H. Wen, H.C. Kou, J.S. Li, H. Chang, X.Y. Xue, L. Zhou, Intermetallics 17 (2009) 266–269.
[11] C.W. Tsai, Y.L. Chen, M.H. Tsai, J.W. Yeh, T.T. Shun, S.K. Chen, J. Alloys Compd. 486 (2009) 427–435.
[12] Y.P. Wang, B.S. Li, M.X. Ren, C. Yang, H.Z. Fu, Mater. Sci. Eng. A 491 (2008) 154–158.
[13] F.J. Wang, Y. Zhang, Mater. Sci. Eng. A 496 (2008) 214–216.
[14] Y.J. Zhou, Y. Zhang, T.N. Kim, G.L. Chen, Mater. Lett. 62 (2008) 2673–2676.
[15] K.B. Zhang, Z.Y. Fu, J.Y. Zhang, W.M. Wang, H. Wang, Y.C. Wang, Q.J. Zhang, J. Shi, Mater. Sci. Eng. A 508 (2009) 214–219.
[16] T.T. Shun, Y.C. Du, J. Alloys Compd. 478 (2009) 269–272.
[17] B.D. Cullity, S.R. Stock, Elements of X-Ray Diffraction, third ed., Prentice-Hall Inc., New Jersey, 2001.
[18] F.R. De Boer, R. Boom, W.C.M. Mattens, A.R. Miedema, A.K. Niessen, Cohesion in Metals, North-Holland, Amsterdam, 1989.
[19] T.T. Shun, Y.C. Du, J. Alloys Compd. 479 (2009) 157–160.
[20] C.T. Sims, N.S. Stoloff, W.C. Hagel, Superalloys II, Wiley, New Jersey, 1987.